Inverse inference of a quantum spin glass

Author: Lluís Torres Hugas*
Màster en Física dels Sistemes Complexos i Biofísica.
Facultat de Física, Universitat de Barcelona, Martí i Franquès 1, 08028 Barcelona, Spain.†

Advisor: Matteo Palassini
Facultat de Física, Departament de Física de la Matèria Condensada, Universitat de Barcelona, Martí i Franquès 1, 08028 Barcelona, Spain.

(Dated: June 30, 2023)

Abstract: In statistical physics, inverse problems arise when we need to design a many-body system with particular desired properties. Rather than calculating observables based on known model parameters, inverse problems involve inferring the parameters of a model based on observations. In my final degree project, we studied the inverse problem for the Viana-Bray spin glass model with a discrete distribution of the couplings, and with simulated annealing, we tried to infer the couplings of the system with the maximum pseudolikelihood method. In this project, we studied the inverse problem for the *quantum* Viana-Bray spin glass model with the same coupling distribution. The goal was to extend the pseudolikelihood maximization approach to a quantum spin glass with a transverse field since most research efforts have focused on the classical version and hardly anything is known about its quantum counterpart. To achieve this, we generated equilibrium configurations from the quantum partition function using quantum Monte Carlo techniques, and then we employed simulated annealing to maximize the pseudolikelihood function and infer the couplings of the system. We derived a modified version of the pseudolikelihood function from the initial proposal after closely following the approach used in the classical case. We found that when introducing the transverse field in the system, the algorithm was still able to infer the couplings; however, because of how the quantum system is treated, certain modifications had to be made to the pseudolikelihood method. Moreover, as in the classical case, we found that the algorithm performed the best around the phase transition boundaries.

I. INTRODUCTION

The transverse-field Ising model (TFIM) was originally introduced during the early 1960s as a theoretical framework to investigate the order-disorder transitions observed in double-well ferroelectric systems, such as in potassium dihydrogen phosphate [1]. With this model, one can map the two states of the double-well potential, representing the proton positions, with the up and down states of a spin, and the tunnelling effect caused by the quantum fluctuations can be mapped to the effect of a transverse field in the spin picture.

It is one of the simplest models to exhibit a zero-temperature quantum phase transition driven by the quantum fluctuations due to the transverse field [2].

The Hamiltonian for this quantum spin system is given by

$$\hat{H}_{\boldsymbol{J}}(\hat{\boldsymbol{\sigma}}) = -\sum_{\langle ij\rangle} J_{ij}\hat{\sigma}_i^z\hat{\sigma}_j^z - \Gamma\sum_{i=1}^{N}\hat{\sigma}_i^x \tag{1}$$

where N is the number of spins, $\boldsymbol{J} = \{J_{ij}\}_{i,j=1,\dots,N}$ are the pairwise couplings, Γ is the transverse field, $\hat{\boldsymbol{\sigma}} = \{\hat{\sigma}_i^x, \hat{\sigma}_i^z\}_{i=1,\dots,N}$ are the $\frac{1}{2}$-spin Pauli matrices and the sum $\sum_{\langle ij\rangle}$ extends over pairs of interacting spins.

Over the past few decades, there has been extensive research dedicated to studying the properties of phases in many-body systems driven by quantum fluctuations, employing a wide range of analytical techniques, including renormalization-group analysis, mean-field approximation, effective-field theory, and perturbation theory, as well as numerical methods such as exact diagonalization, quantum Monte Carlo simulations, and density-matrix renormalization-group calculations [2].

* lltorreh7@alumnes.ub.edu
† master.complex.biophys@ub.edu

Although no general theory has been settled yet, several studies have successfully obtained phase diagrams for specific cases using various approximations. For instance, one of the most straightforward cases is the TFIM on a fully connected graph with $J_{ij} = 1$ (ferromagnetic model), where, under the Bragg-Williams mean-field approximation, the phase boundary is given by the self-consistent equation $\Gamma/J = \tanh \beta\Gamma$ where $\beta = 1/k_B T$ is the inverse temperature, and J is the magnitude of the pairwise couplings [3]. (From now on, we choose units such that $k_B = 1$)

Another model of particular interest within this framework is the quantum spin glass, in which J_{ij} are quenched random couplings that can take both signs. A spin glass (SG) phase occurs due to the competing interactions, where the magnetic moments tend to arrange into specific equilibrium orientations, yet the system does not present magnetic long-range order.

This SG phase was characterized by Parisi [4] with the introduction of a new order parameter when studying the replica symmetry breaking of the classical Sherrington-Kirkpatrick (SK) spin glass model [5], given by Eq. (1) with $\Gamma = 0$ on a fully connected graph, with $\overline{J_{ij}} = 0$ and Var $J_{ij} \propto 1/N$. This order parameter corresponds to the overlap between the spins of two system replicas α and β with the same $\boldsymbol{J}$,

$$q_{\alpha\beta} = \frac{1}{N} \sum_{i=1}^{N} \sigma_{i,\alpha}^{z} \sigma_{j,\beta}^{z}. \tag{2}$$

The spin glass phase is characterized by $\langle q_{\alpha\beta} \rangle \neq 0$ and the paramagnetic phase by $\langle q_{\alpha\beta} \rangle = 0$.

The quantum SK spin glass model has been widely studied both analytically [6–9] and numerically [10–12] however there are still many unanswered questions on its equilibrium and dynamical properties. From these studies, it seems that the zero-temperature critical transverse field is around $\Gamma_c = 1.5J$, where J^2/N is the variance of the distribution of the interaction spins. The current understanding of its phase diagram is shown in Fig. 1.

The advent of quantum annealers (QA) based on quantum adiabatic optimization techniques [13] has

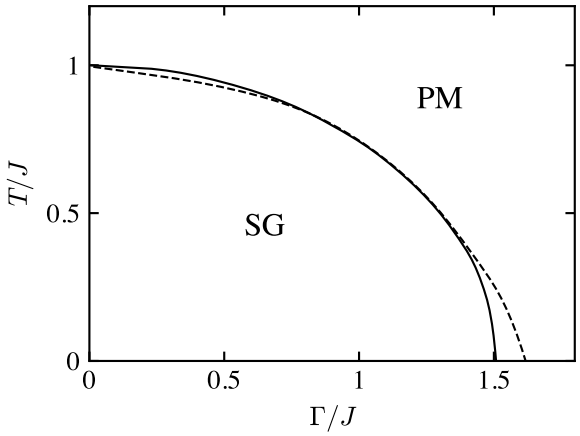

FIG. 1. Phase diagram of the quantum SK spin glass model from different approximations: dashed curve from [8] and solid line from [12]. The phases are spin glass (SG) and paramagnetic (PM).

opened up new avenues for studying these systems. The first somewhat useful programmable commercial devices that attempt to exploit this are the D-Wave One and Two QA [14]. The native benchmark for these QA is a quantum SG; therefore, research on the TFIM is very active today.

One interesting study carried out on these devices is [15], where Harris *et al.* embedded a TFIM on a three-dimensional simple cubic lattice model on a D-Wave quantum processing unit, which allowed a direct observation of the quantum phase transition and the construction of a precise phase diagram.

The usual goal in classical and quantum statistical mechanics is to derive the observable quantities from an appropriate physical model. For example, deriving the spin magnetizations and correlations by starting with a model that describes the interactions between spins.

Instead, one could consider as the starting point the set of observations of some system whose microscopic parameters are unknown and yet to be discovered. In that scenario, we talk about the *inverse problem*, where the goal is to infer the parameters describing the system (for example, its Hamiltonian) from existing data.

During the last years, with the rise of 'big-data' in different fields, for example in high-throughput experiments in biology, the study of inverse problems in statistical physics has gained attention [16].

For the classical SG model, where the inverse problem consists in inferring the couplings $\boldsymbol{J}$ from a set of equilibrium spin configurations, a wide variety of methods have shown some acceptable performance in some temperature ranges [16], where the one that outperformed the rest was the pseudolikelihood (PL) method [23] (see Section III). However, when it comes to the inference of the couplings in the quantum model, hardly anything is known.

In my final degree project [17] we employed the PL method to address the inverse problem of the Viana-Bray (VB) spin glass model [18] with the novelty of a discrete distribution for the couplings.

In this project, we aim to study the quantum counterpart of the same model to analyse whether the performance of the PL method is altered when a transverse field is introduced.

II. INVERSE PROBLEM OF THE QUANTUM VIANA-BRAY SPIN GLASS MODEL

The quantum VB spin glass model consists of a spin glass system on an Erdös-Rényi random graph [19] under the Hamiltonian in Eq. (1). With N nodes and M randomly assigned edges, we can define the average node connectivity as $\langle z\rangle = 2M/N$. As we did in [17], we assign at random to each edge a pairwise coupling J_{ij} following the discrete distribution

$$P(J_{ij}) = p\cdot\delta(J_{ij}-1) + (1-p)\cdot\delta(J_{ij}+1) \qquad (3)$$

where p is the fraction of ferromagnetic ($J_{ij}=1$) interactions. Fig. 2 shows the phase diagram of the model for $\Gamma = 0$.

To perform simulations in a conventional computer and use the typical Monte Carlo methods to study statistical models, there exist a helpful mapping of the TFIM in d-dimensions to an effective d+1-dimensional classical Hamiltonian using the Suzuki-Trotter formalism [21] (see Appendix B).

This formalism has been widely adopted and established as a reliable approach in numerous numerical studies of the TFIM [10, 11].

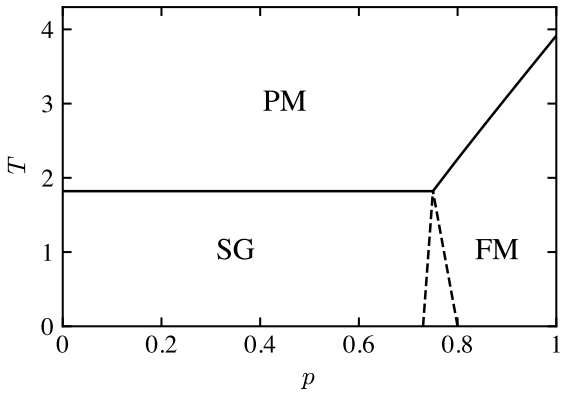

FIG. 2. Phase diagram of the classical VB spin glass model with the discrete distribution of Eq. (3), as determined in [17] from both [18] and [20] for $\langle z\rangle = 4$. The phases are spin glass (SG), ferromagnetic (FM) and paramagnetic (PM). Solid lines correspond to the PM-SG and PM-FM boundaries, and dashed lines delimit the mixed phase between SG and FM.

For Eq. (1), the effective classical Hamiltonian is

$$H^{\boldsymbol{J}}_{\text{eff}}(\boldsymbol{\sigma}) = -\frac{1}{m}\sum_{\alpha=1}^{m}\sum_{\langle ij\rangle} J_{ij}\sigma_i^\alpha\sigma_j^\alpha - K_2\sum_{\alpha=1}^{m}\sum_{i=1}^{N}\sigma_i^\alpha\sigma_i^{\alpha+1} \qquad (4)$$

where $K_2 = -\frac{1}{2\beta}\ln\tanh\frac{\beta\Gamma}{m}$ and $\boldsymbol{\sigma} = \{\sigma_i^\alpha\}_{i=1,\dots,N}^{\alpha=1,\dots,m}$ are Ising $\frac{1}{2}$-spins.

For $m\to\infty$ the equivalence is exact, yet for practical purposes m has to be finite, in that case we talk about the m-th Trotter approximation. This new system can be viewed as having m identical spin systems overlayed and interconnected with an interlayer interaction K_2, with periodic boundaries ($\sigma_i^{m+1} = \sigma_i^1$), see Fig. 3.

For $\Gamma\to 0$, the layers become completely correlated, and the system behaves as a classical spin glass. For $\Gamma\to\infty$, the layers become decoupled, and quantum fluctuations will dominate in the system.

In order to prepare the inverse problem, we generate a set of random graphs with their couplings in the ensemble described above and prepare for each, using Monte Carlo simulations, a sample of C equilibrium configurations $\{\boldsymbol{\sigma}^\mu\}_{\mu=1,\dots,\text{C}}$ following the classical Boltzmann distribution

$$P(\boldsymbol{\sigma}) = \frac{1}{Z(\boldsymbol{J})}\exp\big(-\beta H^{\boldsymbol{J}}_{\text{eff}}(\boldsymbol{\sigma})\big) \qquad (5)$$

where $Z(\boldsymbol{J}) = \sum_{\boldsymbol{\sigma}} \exp(-\beta H^{\boldsymbol{J}}_{\text{eff}}(\boldsymbol{\sigma}))$ is the partition function.

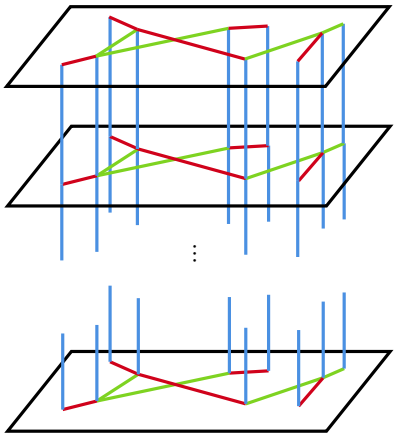

FIG. 3. Schematic representation of the effective classical system we will study. Each layer contains the random graph we want to infer, green and red lines represent the intralayer ferromagnetic and antiferromagnetic interactions, and the blue ones represent the interlayer interactions.

The goal is to study how well we can recover the graph structure and its couplings $\boldsymbol{J}$ from the $\{\boldsymbol{\sigma}^{\mu}\}$ using the PL method.

III. THEORETICAL APPROACH

Since the PL is the best performing method in the classical case, and to establish a meaningful comparison with the classical results reported in [17], we have chosen it for this project too.

As no previous applications of the PL method to quantum systems exists, to our knowledge, we will initially follow closely the classical case. This involves treating the quantum system using the effective classical Hamiltonian and applying the PL method accordingly.

Below we describe first the maximum likelihood method and then the maximum pseudolikelihood method, which is a computationally simpler approximation to the first, both adapted to the quantum case.

A. Maximum Likelihood

An important method for solving statistical inference problems is maximum likelihood (ML) estimation. For a set of observations $x_1, x_2, ...x_{\text{C}}$ obtained from the known distribution $p(x_1, x_2, ...x_{\text{C}}|\theta)$ of a statistical model that depends on a set of parameter θ, one defines the ML estimator to infer the unknown θ from the observations as

$$\theta^{\text{ML}} = \text{argmax}_{\theta}\, p(x_1, x_2, ...x_{\text{C}}|\theta) \tag{6}$$

which is the estimator with the least mean-squared error, and for large C it converges in probability to the original θ.

To avoid working with large numbers, one usually maximizes the logarithm of $p(x_1, x_2, ...x_{\text{C}}|\theta)$.

For our inverse problem, where the observations are $D = \{\boldsymbol{\sigma}^{\mu}\}_{\mu=1,...,\text{C}}$, the unknown parameters are $\boldsymbol{J}$ and assuming the C configurations independently sampled from the Boltzmann distribution Eq. (5), the log-likelihood is

$$L_D(\boldsymbol{J}) = \frac{1}{\text{C}} \ln p(D|\boldsymbol{J}) = \frac{\beta}{m} \sum_{\alpha=1}^{m} \sum_{i<j} J_{ij} \langle \sigma_i^{\alpha} \sigma_j^{\alpha} \rangle_D + \beta K_2 \sum_{i=1}^{m} \sum_{i} \langle \sigma_i^{\alpha} \sigma_i^{\alpha+1} \rangle_D - \ln Z(\boldsymbol{J}) \tag{7}$$

where $\langle Q(\boldsymbol{\sigma}) \rangle_D = \frac{1}{\text{C}} \sum_{\mu} Q(\boldsymbol{\sigma})$ are averages of the function $Q(\boldsymbol{\sigma})$ of spin variables over the observed data. Then, the ML estimator is

$$\boldsymbol{J}^{\text{ML}} = \text{argmax}_{\boldsymbol{J}}\, L_D(\boldsymbol{J}), \tag{8}$$

which can be found by imposing

$$\frac{\partial L_D}{\partial J_{ij}} = \frac{\beta}{m} \sum_{\alpha=1}^{m} \left[\langle \sigma_i^{\alpha} \sigma_j^{\alpha} \rangle_D - \langle \sigma_i^{\alpha} \sigma_j^{\alpha} \rangle \right] = 0 \tag{9}$$

where we used

$$\frac{\partial}{\partial J_{ij}} \ln Z = \frac{\beta}{m} \sum_{\alpha=1}^{m} \langle \sigma_i^{\alpha} \sigma_j^{\alpha} \rangle, \tag{10}$$

and $\langle \sigma_i^{\alpha} \sigma_j^{\alpha} \rangle$ are the expectation values under the Boltzmann distribution.

In principle, since the log-likelihood is known to be concave, one could reach the maximum with

a gradient descent algorithm, such as Boltzmann machine learning [22], where one updates the couplings at each step of the algorithm according to

$$J_{ij}^{n+1} = J_{ij}^{n} + \eta \frac{\partial L_D}{\partial J_{ij}}(\boldsymbol{J}^n) \tag{11}$$

where η is the learning rate of the algorithm, which has $\langle \sigma_i^\alpha \sigma_j^\alpha \rangle_D = \langle \sigma_i^\alpha \sigma_j^\alpha \rangle$ as its fixed point.

However, in order to calculate the expectation values, we would have to compute averages over 2^{Nm} configurations, which is generally intractable. Besides, in our problem, since we work with discrete couplings, this approach is not possible.

B. Maximum Pseudolikelihood

The pseudolikelihood is an alternative to the likelihood function, introduced in 1974 by Besag [23]. This estimator also leads to the exact inference of the model parameters in the $\mathrm{C} \to \infty$ limit. Moreover, it has a more feasible computational complexity that scales polynomially with the size of the sample C, and the size of the system mN. Therefore, it is usually much faster than the exact maximization of the likelihood.

To deduce it, we will adapt the derivation in [16] to our Hamiltonian. To start with, we consider how the statistics of a particular spin variable σ_i^α depends on the configuration of the rest. For that, we split the Hamiltonian as

$$H_{\text{eff}}(\boldsymbol{\sigma}) = H_i^\alpha(\boldsymbol{\sigma}) + \tilde{H}(\boldsymbol{\sigma} \backslash \sigma_i^\alpha) \tag{12}$$

such that the first term $H_i^\alpha(\boldsymbol{\sigma}) = -h_i^\alpha \sigma_i^\alpha$, where we introduced the local field

$$h_i^\alpha = \frac{1}{m} \sum_{j \in V(i)} J_{ij} \sigma_j^\alpha + K_2(\sigma_i^{\alpha+1} + \sigma_i^{\alpha-1}), \tag{13}$$

depends on the couplings of the spin σ_i^α to its neighbours, and the second term $\tilde{H}(\boldsymbol{\sigma} \backslash \sigma_i^\alpha)$ does not depend on σ_i^α. $V(i)$ denotes the set of intralayer neighbours of the i-th spin, and $\boldsymbol{\sigma} \backslash \sigma_i^\alpha$ means all spin variables except σ_i^α.

Using Eq. (12), we can work out the following identity for the expectation value:

$$\begin{aligned}
\langle \sigma_i^\alpha \sigma_j^\alpha \rangle &= \frac{1}{Z(\boldsymbol{J})} \sum_{\boldsymbol{\sigma} \backslash \sigma_i^\alpha} e^{-\beta \tilde{H}} \sum_{\sigma_i^\alpha} \sigma_i^\alpha \sigma_j^\alpha e^{-\beta H_i^\alpha} \\
&= \frac{1}{Z(\boldsymbol{J})} \sum_{\boldsymbol{\sigma} \backslash \sigma_i^\alpha} e^{-\beta \tilde{H}} \sigma_j^\alpha 2 \sinh(\beta h_i^\alpha) \\
&= \frac{1}{Z(\boldsymbol{J})} \sum_{\boldsymbol{\sigma} \backslash \sigma_i^\alpha} e^{-\beta \tilde{H}} \sigma_j^\alpha \tanh(\beta h_i^\alpha) \sum_{\sigma_i^\alpha} e^{-\beta H_i^\alpha} \\
&= \langle \sigma_j^\alpha \tanh(\beta h_i^\alpha) \rangle.
\end{aligned} \tag{14}$$

The key step, and the only approximation involved in going from the ML to the PL, is to change the averages $\langle \sigma_i^\alpha \sigma_j^\alpha \rangle$ and $\langle \sigma_j^\alpha \tanh(\beta h_i^\alpha) \rangle$ over the Boltzmann distribution with the sample means

$$\langle \sigma_i^\alpha \sigma_j^\alpha \rangle_D = \langle \sigma_j^\alpha \tanh(\beta h_i^\alpha) \rangle_D. \tag{15}$$

With this, we have broken down the problem of estimating the full coupling matrix into separate problems of estimating the single row J_{i*} of the coupling matrix for a specific spin σ_i^α using the sampled spin configurations.

The statistics of σ_i^α conditioned on the remaining spins $\{\sigma_j^\delta\}_{j \neq i}^{\delta \neq \alpha}$ can be written as

$$\begin{aligned}
p\left(\sigma_i^\alpha | \{\sigma_j^\delta\}_{j \neq i}^{\delta \neq \alpha}\right) &= \frac{e^{-\beta H_i^\alpha}}{\sum_{\sigma_i^\alpha} e^{-\beta H_i^\alpha}} = \frac{e^{\beta h_i^\alpha \sigma_i^\alpha}}{e^{\beta h_i^\alpha \sigma_i^\alpha} + e^{-\beta h_i^\alpha \sigma_i^\alpha}} \\
&= \frac{1}{2}\left(1 + \sigma_i^\alpha \tanh \beta h_i^\alpha\right).
\end{aligned} \tag{16}$$

Considering we have m layers, the log-likelihood for the i-th row of couplings J_{i*} is

$$L_D^i(J_{i*}) = \frac{1}{m} \sum_{\alpha=1}^{m} \frac{1}{C} \sum_{\mu} \ln \frac{1}{2}\left(1 + \sigma_i^{\alpha,\mu} \tanh \beta h_i^{\alpha,\mu}\right). \tag{17}$$

Finally, we sum over all the J_{i*} and obtain the log-pseudolikelihood

$$PL_D(\boldsymbol{J}) = \sum_{i=1}^{N} L_D^i(J_{i*}). \tag{18}$$

In the classical case, the maximization of this function is one of the most efficient ways to solve the inverse problem [16].

IV. COMPUTATIONAL APPROACH

A. Sample Preparation

In order to generate the samples $\boldsymbol{\sigma}^{\mu}$ we use the Metropolis Markov Chain Monte Carlo algorithm [24]. In spin systems, one usually starts with a random configuration of the spins, and by proposing single spin flips with the normalized acceptance probability $\min(1, e^{-\beta\Delta H_{\text{eff}}})$, where ΔH_{eff} is the energy difference resulting from the spin flip, one can generate equilibrium configurations after some equilibration time.

With our effective Hamiltonian, Eq. (4), the nearest neighbour (intralayer) interactions remain the same as in the original quantum Hamiltonian with an extra $1/m$ factor, while the transverse field (interlayer) interaction K_2 is non-trivially dependent on thermodynamic variables. Then, the acceptance probability will be highly conditioned by the different ranges of the temperature and the transverse field, and thereby the sample generation may be affected.

In Fig. 4 we can see that the interlayer interaction is significantly larger than the intralayer interaction, except at very low temperatures. This means that when proposing a single spin flip, its acceptance will primarily depend on the interlayer term.

When $\Gamma \to 0$, we anticipate the system to behave as in the classical model. In the Suzuki-Trotter formalism, this means that all the layers should be identical, and the world-lines $\sigma_i = \{\sigma_i^{\alpha}\}_{\alpha=1,\dots,m}$ should behave as the spins in the classical system.

At low Γ, when starting from a random configuration of the system, spins in the same world-line will rapidly align due to the strong interlayer interaction K_2. Once this alignment is settled, the system becomes frozen because accepting a spin flip would incur a high energy cost. However, this frozen state does not necessarily ensure that the world-lines are in the most energetically stable orientation for the intralayer interactions. This is problematic because, in order to capture the classical behaviour, the intralayer interactions should govern the state of the system in this situation. The above problem can be solved by introducing world-line flips. Instead of only proposing single spin flips at each Monte Carlo step, we randomly chose between flipping one spin σ_i^{α} or flipping a world line σ_i.

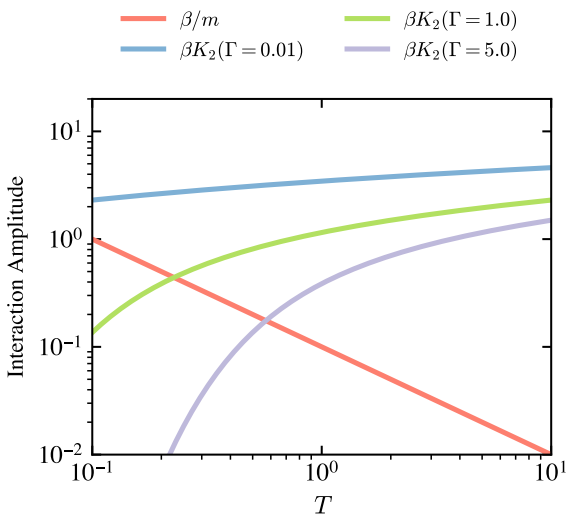

FIG. 4. Dependence of the two interaction terms amplitudes of $\beta\Delta H_J^{\text{eff}}$ as a function of the temperature for different values of the transverse field Γ on a log-log scale. $m = 10$ for both terms.

In world-line flips there is no interlayer contribution in the energy difference,

$$\Delta E(\sigma_i \to -\sigma_i) = \frac{2}{m} \sum_{\alpha=1}^{m} \sigma_i^{\alpha} \sum_{j \in V(i)} J_{ij} \sigma_j^{\alpha}, \qquad (19)$$

therefore the acceptance probability will only be given by the intralayer term. This property enables the system to reach equilibrium for all possible values of the transverse field, which is key for generating good equilibrium samples that serve as the starting point for the inverse problem.

B. Simulated Annealing

As previously mentioned, our objective is to maximize Eq. (18). For that, we will employ simulated annealing (SA) [25], a stochastic global optimization algorithm. SA is a partial search algorithm, which means that it does not guarantee to provide the absolute best solution to the problem but rather an approximation due to computational or information limitations. Nonetheless, it is

well-suited for our problem, characterized by a high-dimensional, discrete search space with many local optima. Its ability to navigate such complex landscapes and explore a wide range of solutions without getting stuck in a local maxima makes it a good choice.

SA is based on introducing a fictitious temperature T_F in the search space and sampling from $\exp(\Delta PL_D/T_F)$ by the Metropolis algorithm. The initial step is selecting a random point in the search space, that is to say, a random graph with a random assignment of the couplings following the distribution of Eq. (3). Then we perform a finite number τ of Monte Carlo steps (MCS), each of which consists in M random exchanges between pairs of couplings of the initial graph. These exchanges can either relocate one edge of the graph to a different position or substitute a ferromagnetic edge with an antiferromagnetic one, see Fig. 5.

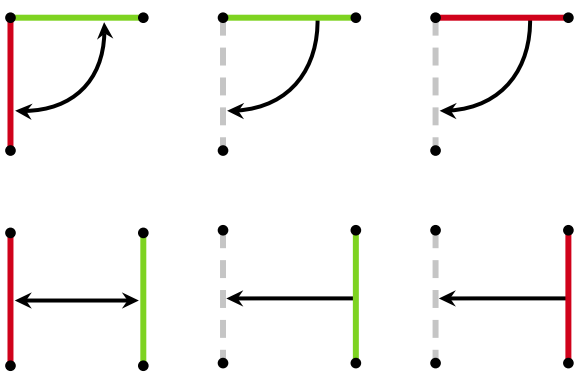

FIG. 5. Schematic representation of the possible exchanges and relocations of edges in the SA algorithm. Black dots represent the positions of spins, while green and red lines represent ferromagnetic and antiferromagnetic couplings, respectively. Dashed gray lines represent the absence of a coupling.

Each exchange is accepted with a probability given by $\min(1, \exp(\Delta PL_D/T_F))$, where ΔPL_D is the variation of the log-PL due to the exchange of the coupling.

During the simulation, the fictitious temperature is progressively reduced following the cooling schedule

$$T_F(t) = T_F^{\text{ini}} \left(1 - \frac{t}{\tau}\right) \tag{20}$$

where t is the current simulation time in MCS units, and T_F^{ini} is the initial fictitious temperature, which is set relatively high, allowing for a broader exploration of the search space.

As the simulation progresses and the temperature decreases, the search space becomes narrower and more focused, helping the algorithm converge towards the global maxima.

C. Relative Reconstruction Error

To explore how the algorithm performance depends on the different parameters of the system, we define the relative reconstruction error as a quantitative measure of the degree of similarity between the reconstructed couplings $\boldsymbol{J}^{\text{PL}} = \{J_{ij}^{\text{PL}}\}$ and the original system couplings $\boldsymbol{J} = \{J_{ij}\}$:

$$\gamma = \frac{1}{M} \sum_{i<j} (J_{ij} - J_{ij}^{\text{PL}}) \tag{21}$$

A value of $\gamma = 0$ would mean that $\boldsymbol{J} = \boldsymbol{J}^{\text{PL}}$, *i.e.* the reconstruction was perfect, and a value of $\gamma = 1$ would mean that none of the couplings has been correctly reconstructed.

The phase space of our system is characterized by three thermodynamic quantities: the temperature T, the transverse field Γ and the parameter p that rules the couplings distribution. In order to assess the accuracy of the reconstruction algorithm for different (T, Γ, p), it is essential to obtain statistically representative results. This means that we have to average the algorithm's performance over a sufficiently large and diverse set of graphs.

V. PREVIOUS RESULTS

Previously, in [12] we addressed the inverse problem for the classical VB spin glass model ($\Gamma = 0$) with the same distribution for the couplings. Below we summarize our main results.

We first considered 100 random graphs of $N = 100$ and $\langle z \rangle = 4$ with $p = 0.50$ and $T = 1.0$, and studied how the simulations parameters C, τ or T_F^{ini} affect the algorithm performance.

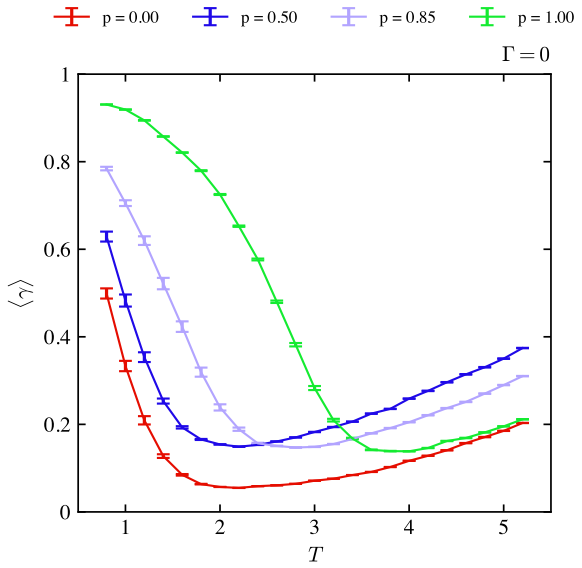

FIG. 6. Relative reconstruction error for the classical VB spin glass as a function of the temperature with $N = 100$ and $\langle z \rangle = 4$, for different values of the parameter p. The error bars correspond to the standard deviation of the mean value, calculated from a set of 100 graphs.

We found that increasing C and τ always improves the performance. However, this comes with a computational cost, and the improvement when these values are already large is not very significant. We found that for C = 400 and $\tau = 2000$ the balance between accuracy and affordable computational time was reasonable. The initial fictitious temperature T_F^{ini}, has an optimal value that depends on the real temperature T. Based on the form of the log-PL and different adjustments, we found that a good choice was

$$T_F^{\text{ini}}(T) = -\frac{1}{\langle z \rangle} \ln \left[\frac{1}{2} \left(1 + \tanh \frac{1}{T} \right) \right]. \qquad (22)$$

In order to test the reproducibility of the algorithm, we performed 100 different runs over the same system with the same thermodynamic and simulation parameters to see how the different values of γ were distributed. The results suggested that, since the distribution of the values was very narrow, one run is representative of how the algorithm performs on that specific system.

With all the aforementioned optimizations, we evaluated the algorithm's performance as a function of p and T.

In Fig. 6 we show how the relative reconstruction error depends on the temperature, for different values of p. Each point corresponds to the average of over 100 graphs in the ensemble. Notice that for each p, there is a minima in the error curve.

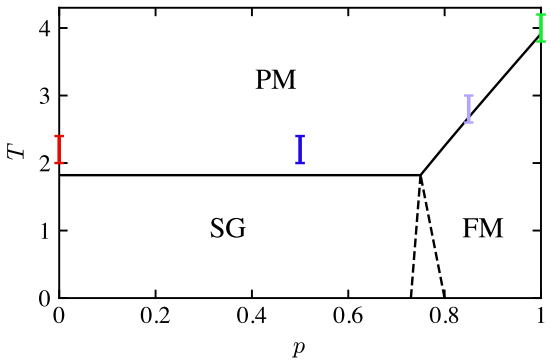

FIG. 7. Phase diagram for the classical VB spin glass model with the discrete distribution of Eq. 3. $T = \beta^{-1}$ and $\langle z \rangle = 4$. The phases are: PM paramagnetic, FM ferromagnetic, and SG spin-glass. Solid lines correspond to the PM-SG and PM-FM boundaries, and dashed lines delimit the mixed phase between SG and FM. The coloured points correspond to the best performing temperature value from Fig. 6. The color of each point is chosen just to match the color associated with the parameter p used in Fig. 6.

In Fig. 7 we represent the position of the minimum for each p value together with the phase diagram of this model, Fig. 2.

The best-performing range is around the phase transition temperatures, both FM-PM and SG-PM. In this case, the temperature is not high enough to dominate the system and remove the couplings relevance, but high enough to allow the system to explore a larger part of the phase space, which will generate samples that contain relevant information on how the spins interact with each other, allowing good reconstructions.

Another point worth mentioning is that the phase

diagram of this system is qualitatively the same for different values of $\langle z \rangle$. Hence, the behaviour obtained in the relative reconstruction error would be similar, but with the respective shift of the best-performing temperature to the corresponding critical temperature.

VI. RESULTS

We now present how the maximum PL performs on the quantum VB spin glass model with discrete couplings using the 10-th Trotter approximation ($m = 10$).

As in the classical case, we are going to perform this study by averaging 100 graphs for each value of p with $N = 100$ and $\langle z \rangle = 4$, with simulation parameters $C = 400$, $\tau = 2000$ and T_F^{ini} given by Eq. (22).

A. log-PL maximization

Before discussing the simulation results, we put forth the following argument.

At very low Γ one could expect that the results will be comparable to the classical counterpart since quantum effects are mild, and each configuration will consist of m copies of the same classical configuration. Consequently, when computing the log-PL, these copies contribute additional irrelevant averages that should not significantly impact the reconstruction process.

As the transverse field is increased, the system experiences an enhanced presence of quantum fluctuations. This, in turn, leads to a decrease in the critical temperatures for the transitions from SG to PM and from FM to PM. This phenomenon should be reflected in the performance as a shift in the optimal temperature downward.

Upon examining Fig. 8, where we show how the relative reconstruction error depends on the temperature for two different values of Γ, it becomes evident that the observed behaviour does not align with the above expectation. For low Γ, the results are poor, and the curve bears no resemblance to the classical one, Fig. 6. At high Γ, the results show some improvement at low temperatures, but the relative reconstruction error remains generally high.

We explain this with the dominance of the term K_2 in the local field in Eq. (13), which creates a flattened landscape in the search space during the maximization of the log-PL. As a result, the presence of different hills, which encode the system structure through the first term of the local field, becomes less significant when seeking the maximum value. However, when the transverse field Γ is high Fig. 8 (b) and the relative magnitudes of the two terms in the local field become more comparable, especially at low temperatures, we observe a significant improvement in the reconstructions.

B. Modified log-PL

Due to the above findings we decided to redefine the local field in the log-PL as

$$\tilde{h}_i^\alpha = \frac{1}{m} \sum_{j \in V(i)} J_{ij} \sigma_j^\alpha, \tag{23}$$

removing the K_2 contribution.

In Fig. 9 we can see that with this revised form of the log-PL we are able to obtain much better results.

Although the relative reconstruction error curve for $\Gamma = 1$ in Fig. 9 (a) shows a similar shape to the classical case in Fig. 6, it is important to note that the reconstructions in the quantum system are of lower quality (higher γ). This can be attributed to the introduction of quantum fluctuations, which have an adverse effect on capturing the intralayer couplings of spins within the sample, making it more challenging to accurately infer and capture the underlying spin interactions.

In the case of $\Gamma = 4$ as shown in Fig. 9 (b), the results exhibit improvements across all temperature ranges when compared to the original formulation with the K_2 term in the local field. This suggests that removing the K_2 term and sacrificing the potential information it could provide to the log-PL maximization process is beneficial, even when the original two terms in the local field are comparable in magnitude. The observed improvements indicate that the negative impact of the K_2 term outweighs any potential benefits it might offer, leading to better overall results.

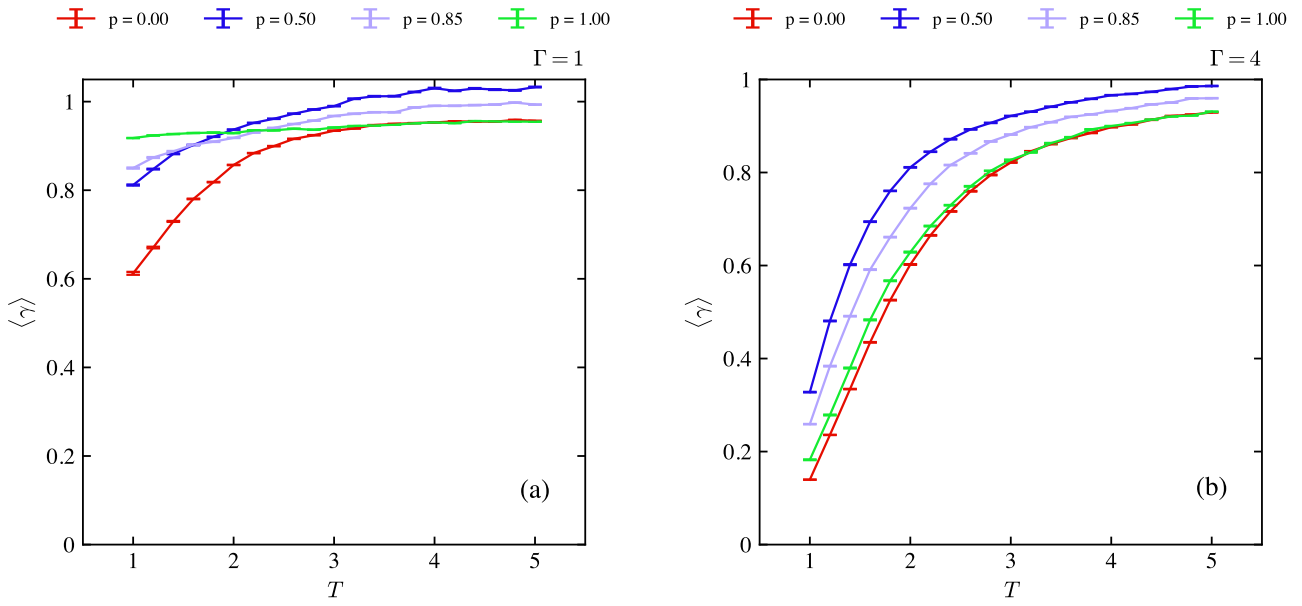

FIG. 8. Relative reconstruction error for the quantum VB spin glass as a function of the temperature with $N = 100$ and $\langle z \rangle = 4$, for different values of the parameter p. (a) with $\Gamma = 1$ and (b) with $\Gamma = 4$. Results using the first log-PL proposed in Eq. (18). The error bars correspond to the standard deviation of the mean value, calculated from a set of 100 graphs with identical p value.

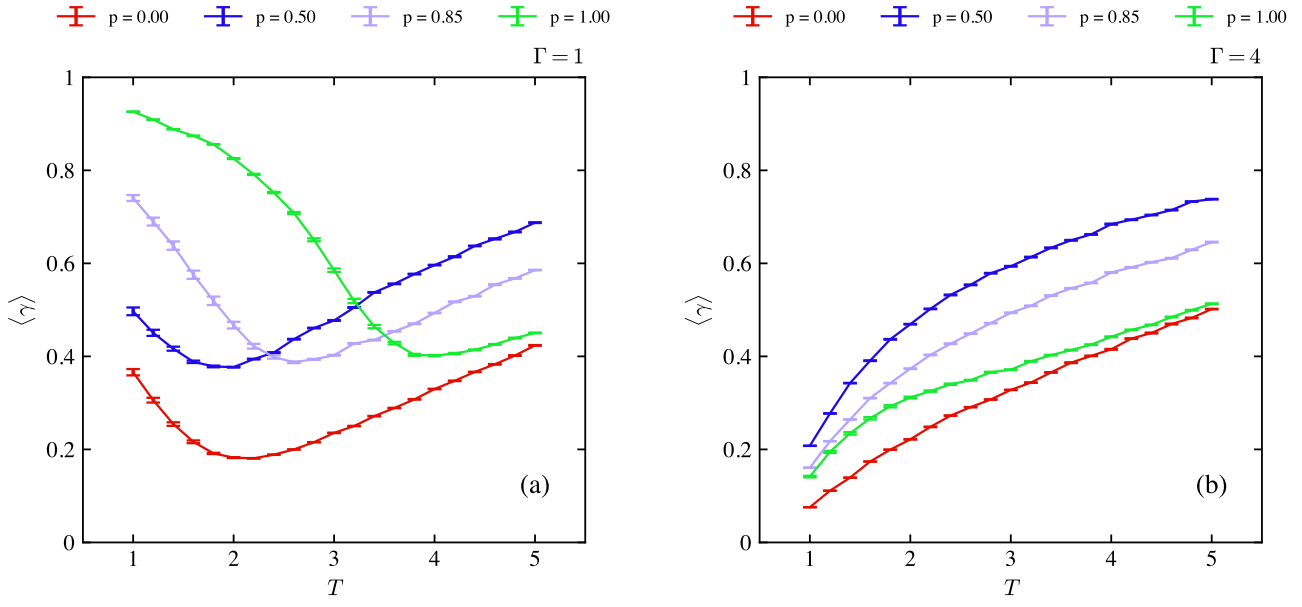

FIG. 9. Relative reconstruction error for the quantum VB spin glass as a function of the temperature with $N = 100$ and $\langle z \rangle = 4$, for different values of the parameter p. (a) with $\Gamma = 1$ and (b) with $\Gamma = 4$. Results using the modified log-PL. The error bars correspond to the standard deviation of the mean value, calculated from a set of 100 graphs with identical p value.

In Appendix C, additional relative reconstruction error results are shown, showcasing the performance for various values of Γ.

C. Phase Diagram and Algorithm Performance

After obtaining the performance results for different values of Γ, the next step is to examine whether the best-performing temperature moves along the phase transition boundary as Γ increases.

In the mean-field approximation of the quantum SK ferromagnetic model, the phase boundary is defined by $\Gamma/J = \tanh \beta\Gamma$ [3]. Both $T_c(0) = J$, the critical temperature at $\Gamma = 0$, and $\Gamma_c(0) = J$, the critical transverse field at $T = 0$, are determined by the parameter J, which represents the magnitude of the couplings.

For the quantum SK spin glass model with Gaussian couplings, different phase boundaries are represented in Fig. 2, giving the critical parameters $T_c(0) = J$ and $\Gamma_c(0) \approx 1.5J$ where J^2/N is the variance of the couplings.

For the quantum VB spin glass model with our discrete distribution, obtaining analytical results is extremely complicated, and the phase boundary is not known.

However, in order to establish a reference line, we make the assumption that in the FM phase the phase boundary of our system has the same shape as the quantum SK ferromagnetic model, but rescaling its critical temperature at $\Gamma = 0$, $T_c(\Gamma = 0, p) = T_c(0, p)$, to the one from the phase diagram with discrete couplings, obtained from Fig. 2. So, we are taking the reference phase boundary given by the following self-consistent equation:

$$\frac{\Gamma}{T_c(0,p)} = \tanh \beta\Gamma. \tag{24}$$

In the SG phase we make the same assumption but rescaling the phase diagram of the quantum SK spin glass model, solid line from Fig. 1, with the respective $T_c(0, p)$ in Fig. 2.

This results in the phase boundaries represented in Fig. 10 for different p.

The results from Fig. 10 demonstrate that, as argued earlier in Section VI A, the best-performing temperature decreases as the transverse field increases. This observation aligns with our previous analysis and supports the notion that the best-performing temperature follows the proposed reference phase boundaries of the system.

This trend maintains the conclusion from the classical system that the best-performing range of temperatures is around the phase transitions, both for the FM-PM and SG-PM.

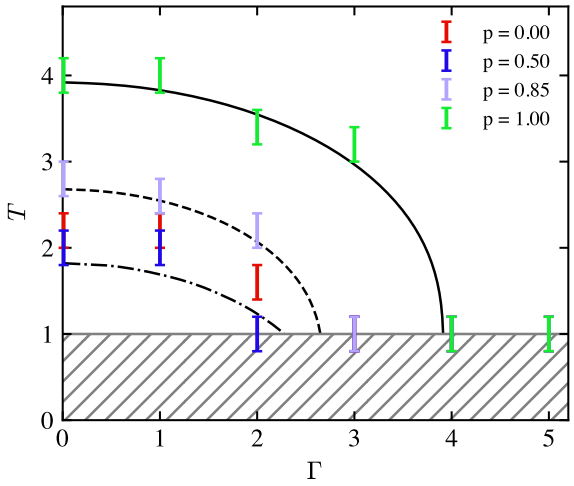

FIG. 10. Best-performing temperature of the quantum VB spin glass model with the discrete distribution of Eq. 3 for different values of p as a function of the transverse field, for $\langle z \rangle = 4$. The lines correspond to different reference phase boundaries: solid and dashed line to the proposed quantum VB ferromagnetic phase boundary with $p = 1$ and $p = 0.85$ respectively, dot dashed line is the quantum SK spin glass model phase boundary rescaled with $T_c(0, p_{\mathrm{SG}})$, where p_{SG} are all the p values in the SG phase of the classical VB spin glass model since they all have the same critical temperature. The gray dashed zone indicates that we are not exploring this temperature range; therefore, the points touching the barrier may not be the actual best-performing temperature.

VII. CONCLUSIONS

In this work, we have conducted extensive studies on generating equilibrium configurations in order to have a good starting point for the inverse problem,

and constructing a reliable log-pseudolikelihood function to correctly infer the underlying parameter of the system. We can now summarise our findings for the inverse problem of the quantum Viana-Bray spin glass.

For the effective classical Hamiltonian, we derived the log-PL function for inferring the pairwise interactions of the underlying graph structure. However, when the interlayer interactions are significantly larger than the intralayer interactions, the dominance of this term in the log-PL function prevented the algorithm from generating accurate reconstructions.

Consequently, we were compelled to redefine the log-PL function by excluding this contribution in order to improve the algorithm performance.

With this new log-PL we achieved significant improvements in the reconstructions. For low values of the transverse field, we were able to reproduce the classical results, but with a general worse quality in the reconstructions. As the transverse field increased, we observed a decrease in the best-performing temperature close to the phase boundary.

This finding aligns with our expectations that the best-performing region on the new phase diagram would still be around the phase transitions, both for the FM-PM and SG-PM, and shows the impact of the quantum fluctuations on the reconstruction process.

ACKNOWLEDGMENTS

I would like to thank my advisor for his guidance and assistance throughout the project, as well as my family and friends for their support.

Appendix A: Code

The source code for the simulations can be found at this link: https://github.com/llui2/TFM_2023

Appendix B: Suzuki-Trotter formalism

Here we show a quick review on how to derive the effective classical Hamiltonian using the Suzuki-Trotter formalism for the TFIM Hamiltonian.

The Trotter formula states that for two not necessarily commuting operators $\hat{A}$ and $\hat{B}$

$$\lim_{n\to\infty}\left(e^{\beta(\frac{\hat{A}}{n}+\frac{\hat{B}}{n})}\right)^n = e^{\beta(\hat{A}+\hat{B})} \tag{B1}$$

Then the derivation of the effective classical Hamiltonian works as follows. We begin with the quantum Hamiltonian,

$$\hat{H} = \hat{H}_D + \hat{V} = -\sum_{i<j} J_{ij}\hat{\sigma}_i^z\hat{\sigma}_j^z - \Gamma\sum_i \hat{\sigma}_i^x. \tag{B2}$$

We chose the following basis of the 2^N Hilbert space,

$$|\boldsymbol{\sigma}\rangle = |\sigma_1\rangle\otimes ...\otimes|\sigma_N\rangle = |\sigma_1^z\rangle\otimes ...\otimes|\sigma_N^z\rangle \tag{B3}$$

where N is the number of spins. Now the partition function, using the Trotter formula, can be written as

$$\begin{aligned} Z &= \mathrm{Tr}\; e^{-\beta\hat{H}} = \mathrm{Tr}\; e^{-\beta(\hat{H}_D+\hat{V})} \\ &= \mathrm{Tr}\lim_{m\to\infty}\left[e^{-\beta(\hat{H}_D/m+\hat{V}/m)}\right]^m \\ &= \lim_{m\to\infty}\mathrm{Tr}\prod_{\alpha=1}^{m} e^{\frac{\beta}{m}\sum_{i<j}J_{ij}\sigma_i^\alpha\sigma_j^\alpha}\langle\boldsymbol{\sigma}^\alpha|e^{\frac{\beta\Gamma}{m}\sum_i\hat{\sigma}_i^x}|\boldsymbol{\sigma}^{\alpha+1}\rangle \end{aligned} \tag{B4}$$

since $\hat{H}_D$ is diagonal in this basis. Now one can easily workout the following expression

$$\langle\boldsymbol{\sigma}^\alpha|e^{\frac{\beta\Gamma}{m}\hat{\sigma}^x}|\boldsymbol{\sigma}^{\alpha+1}\rangle = e^{\frac{1}{2}\ln\left(\sinh\frac{\beta\Gamma}{m}\cosh\frac{\beta\Gamma}{m}\right)-\frac{1}{2}\sigma^\alpha\sigma^{\alpha+1}\ln\tanh\frac{\beta\Gamma}{m}}. \tag{B5}$$

Therefore the m-th Trotter approximation is

$$\begin{aligned} Z \simeq \mathrm{Tr}\Bigg[&\left(\sinh\frac{\beta\Gamma}{m}\cosh\frac{\beta\Gamma}{m}\right)^{\frac{Nm}{2}} \\ &\exp\left(\frac{\beta}{m}\sum_{\alpha=1}^{m}\sum_{i<j}J_{ij}\sigma_i^\alpha\sigma_j^\alpha - \frac{1}{2}\ln\tanh\frac{\beta\Gamma}{m}\sum_{\alpha=1}^{m}\sum_{i=1}^{N}\sigma^\alpha\sigma^{\alpha+1}\right)\Bigg]. \end{aligned} \tag{B6}$$

When m is finite, the exponential of the sum of two non-commutative operators verifies the Baker–Campbell–Hausdorff formula

$$e^{\frac{\beta}{m}(\hat{H}_D+\hat{V})} = e^{\frac{\beta}{m}\hat{H}_D}e^{\frac{\beta}{m}\hat{V}}e^{-\left(\frac{\beta}{m}\right)^2[\hat{H}_D,\hat{V}]+\mathcal{O}(\frac{\beta}{m})^3} \tag{B7}$$

so in order to have a good approximation we have to impose that $\frac{\beta}{m}\ll 1$, in other words that $m\gg\frac{1}{T}$. Usually one takes $m\simeq\frac{10}{T}$.

Appendix C: Relative Reconstructions Error Plots

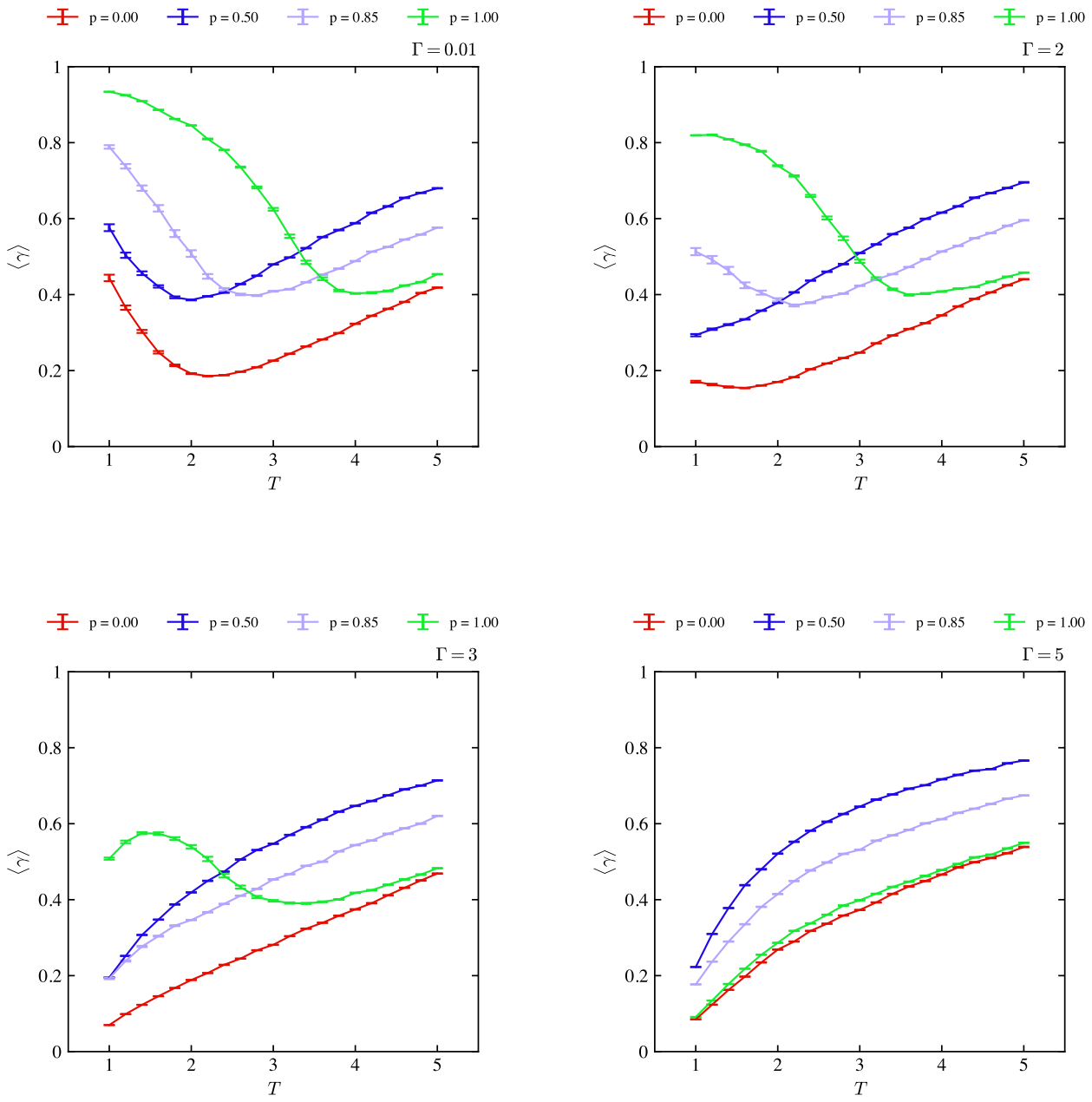

FIG. 11. Relative reconstruction error for the quantum VB spin glass as a function of the temperature with $N = 100$ and $\langle z \rangle = 4$, for different values of the parameter p and different Γ values. Results using the modified log-PL. The error bars correspond to the standard deviation of the mean value, calculated from a set of 100 graphs with identical p value.

[1] R. Blinc. On the isotopic effects in the ferroelectric behaviour of crystals with short hydrogen bonds, *J. Phys. Chem. Solids*, 13(3-4): 204-211, 1960.

[2] S. Suzuki, J.-I. Inoue, and B. K. Chakrabarti. Quantum Ising Phases and Transitions in Transverse Ising Models. *Springer-Verlag Berlin Heidelberg*, 2nd ed., 2013.

[3] R. M. Stratt. Path-integral methods for treating quantal behavior in solids: Mean-field theory and the effects of fluctuations. *Phys. Rev. B*, 33(3): 1921–1930, 1921.

[4] G. Parisi. The order parameter for spin glasses: a function on the interval 0-1. *J. Phys. A: Math. Gen.*, 13(3): 1101–1112, 1980.

[5] D. Sherrington and S. Kirkpatrick. Solvable Model of a Spin-Glass. *Phys. Rev. Lett.*, 35(26): 1792, 1975.

[6] T. Yamamoto and H. Ishii. A perturbation expansion for the Sherrington-Kirkpatrick model with a transverse field. *J. Phys. C: Solid State Phys.*, 20(35): 6053–6060, 1987.

[7] T. K. Kopec. Transverse freezing in the quantum Ising spin glass: a thermofield dynamic approach. *J. Phys. C: Solid State Phys.*, 21(2): 297-307, 1988.

[8] Y. Y. Goldschmidt and P.-Y. Lai. Ising Spin Glass in a Transverse Field: Replica-Symmetry-Breaking Solution. *Phys. Rev. Lett.*, 64(21): 2467–2470, 1990.

[9] P. M. Schindler, T. Guaita, T. Shi, *et al.*. Variational Ansatz for the Ground State of the Quantum Sherrington-Kirkpatrick Model. *Phys. Rev. Lett.*, 129(22): 220401, 2022.

[10] P.-Y. Lai and Y. Y. Goldschmidt. Monte Carlo Studies of the Ising Spin-Glass in a Transverse Field. *Europhys. Lett.*, 13(4): 289–294, 1990.

[11] J. V. Alvarez and F. Ritort. Quantum Monte Carlo study of the infinite-range Ising spin glass in a transverse field. *J. Phys. A: Math. Gen.*, 29(23): 7355–7366, 1996.

[12] A. P. Young. Stability of the quantum Sherrington-Kirkpatrick spin glass model. *Phys. Rev. E*, 96(3): 032112, 2017.

[13] A. B. Finnila, M. A. Gomez, C. Sebenik, *et al.*. Quantum annealing: A new method for minimizing multidimensional functions. *Chem. Phys. Lett.*, 219(5-6): 343-348, 1994.

[14] http://www.dwavesys.com

[15] R. Harris, Y. Sato, A. J. Berkley, *et al.*. Phase transitions in a programmable quantum spin glass simulator. *Science*, 361(6398): 162, 2018.

[16] H. C. Nguyen, R. Zecchina and J. Berg. Inverse statistical problems: from the inverse Ising problem to data science. *Adv. Phys.*, 66(3): 197-261, 2017.

[17] Ll. Torres. Learning Network Structures In Discrete Statistical Models. *Treball de fi de Grau*, 2022.

[18] L.Viana and A.J. Bray. Phase diagrams for dilute spin glasses. *J. Phys. C: Solid State Phys.*, 18(15): 3037–3051, 1985.

[19] P. Erdös and A. Rényi. On Random Graphs. I. *Publ. Math. Debrece*, 6: 290-297, 1959.

[20] M.O. Hase. Spin-glass behaviour on random lattices. *J. Stat. Mech.*, 2012(10): 10007, 2012.

[21] M. Suzuki. Relationship between d-Dimensional Quantal Spin Systems and d+1-Dimensional Ising Systems: Equivalence, Critical Exponents and Systematic Approximants of the Partition Function and Spin Correlations. *Prog. Theor. Phys.*, 56(5): 1454–1469, 1976.

[22] D. H. Ackley, G. E. Hinton, and T. J. Sejnowski. A learning algorithm for Boltzmann machines. *Cogn. Sci.*, 9(1): 147–169, 1985.

[23] J. Besag. Spatial interaction and the statistical analysis of lattice systems. *J. R. Stat. Soc. B*, 36(2): 192–236, 1974.

[24] M. E. J. Newman and G. T. Barkema. Monte Carlo Methods in Statistical Physics. *Oxford University Press*, 2001.

[25] S. Kirkpatrick, C. D. Gelatt Jr and M.P. Vecchi. Optimization by Simulated Annealing. *Science*, 220(4598): 671–680, 1983.